

Cite this: *Energy Adv.*, 2024,  
3, 800

# Life cycle assessment of low-dimensional materials for perovskite photovoltaic cells†

Achyuth Ravilla, <sup>a</sup> Carlo A. R. Perini, <sup>b</sup> Juan-Pablo Correa-Baena, <sup>b</sup>  
Anita W. Y. Ho-Baillie <sup>‡</sup> and Ilke Celik <sup>\*a</sup>

While perovskite solar cells (PSC) have a high potential of achieving commercial-scale manufacturing, they still face some deficiencies regarding rapid degradation in the presence of moisture, oxygen, and high-temperature exposure. To address these challenges, recent research has identified lower dimensional (LD) materials as promising candidates to improve the stability and power conversion efficiency (PCE) of PCSs. The goal of this study is to analyze the environmental performance of LD material-based PSCs (ld-PSC) through a comprehensive life cycle assessment, comparing their environmental performance with reference PSC and commercial photovoltaics (PV) technologies including single-crystalline (c-Si), copper indium gallium diselenide (CIGS) and cadmium telluride (CdTe). To achieve this objective, we evaluated five LD materials such as graphene, reduced graphene oxide (rGO), graphene quantum dots (GQDs), molybdenum disulfide (MoS<sub>2</sub>), and black phosphorus (BP) that are commonly studied in experimental works, and two alternative (Alt) ld-PSC configurations such as Alt-1 and Alt-2, featuring LD materials with lower environmental and comparatively higher among those studied. A comparison of LD materials on a unit mass basis reveals that rGO, graphene, and MoS<sub>2</sub> are the most environmentally friendly options. However, their environmental impact changes significantly when incorporated into ld-PSC configurations based on the type and amount of chemicals used for the dispersion which emphasizes the importance of carefully selecting the chemicals used for dispersion. Our results show that the Alt-1 configuration is ~25% lower and the Alt-2 configuration has ~15% higher average environmental impacts compared to reference PSCs. Further analyses show that at 20% benchmark PCE, ld-PSC has the potential to outperform the environmental performance of all conventional technologies, even with a lifetime up to 2.5 times shorter. Additionally, ld-PSC has a faster energy payback period compared to commercial PV technologies.

Received 6th November 2023,  
Accepted 23rd February 2024

DOI: 10.1039/d3ya00540b

rsc.li/energy-advances

## 1. Introduction

Globally, solar power installations have surged to a remarkable 1.2 TW<sub>dc</sub>, with the United States contributing significantly by reaching 142 GW<sub>dc</sub> installations.<sup>1,2</sup> At present, around 5% of global electricity is generated from solar photovoltaics (PV), and it is expected to make up a significantly higher percentage of global electricity production by the year 2050, with 38%.<sup>3,4</sup> To achieve this goal, large-scale deployment of durable and

efficient solar technologies is required. Currently, >90% of the global PV market is dominated by crystalline silicon solar PVs.<sup>5,6</sup> Among the crystalline silicon PV technologies, the single-crystalline (c-Si) PV technology has reached the highest power conversion efficiency (PCE) rate, 26.1%.<sup>7</sup> There have been significant efforts in recent years to reduce the materials and energy utilization in c-Si synthesis,<sup>8</sup> yet, the processing of the c-Si PV is still expensive and less environmentally friendly compared to thin film PV technologies.<sup>9,10</sup> Among emerging thin-film PV technologies, perovskite solar cells (PSCs) have been recognized as one of the most promising PV technologies with the potential to be a low-cost and environmentally friendly alternative to the c-Si PVs.<sup>9,11–13</sup>

The attention on PSCs over other PV technologies is driven by the favorable combination of high performances, ease of processing, and tunable optical properties offered by the perovskite active layer.<sup>12–14</sup> Such properties make PSCs particularly promising both in single- and multi-junction applications, enabling lower costs and higher energy yields than existing PV

<sup>a</sup> D, department of Civil and Environmental Engineering, Portland State University, Portland, 97201, OR, USA. E-mail: ilke@pdx.edu

<sup>b</sup> School of Material Science and Engineering, Georgia Institute of Technology, Atlanta, 30332, GA, USA

<sup>c</sup> School of Physics and University of Sydney Nano Institute, The University of Sydney, Sydney, NSW 2006, Australia

† Electronic supplementary information (ESI) available. See DOI: <https://doi.org/10.1039/d3ya00540b>

‡ Department of Mechanical and Material Engineering, Portland State University, Portland, 97201, OR, USA.



technologies.<sup>12–19</sup> The best-recorded PCE of single junction PSCs has reached 26.1%, which is equivalent to c-Si PV and perovskite-Si tandem devices have even surpassed 30% PCE.<sup>7</sup> Despite their great potential, PSCs are still limited by poor stability.<sup>20–22</sup> The active layer degrades in the presence of moisture, oxygen, high temperature, or upon reactions with other layers in the stack.<sup>14,23</sup> Halide ions in the perovskite film can react with interlayers and with the metal electrodes, leading to a rapid performance loss.<sup>6,23–25</sup> Previous studies have suggested several approaches to enhance stability and prevent the degradation of PSCs. These include the use of various thin film encapsulation materials, the choice of charge transport layers with large ionization energy and high crystallization temperature, material composition tuning such as converting three-dimensional (3D) perovskite to two-dimensional (2D) perovskite, the passivation of grain boundaries with hydrophobic coatings, and the incorporation of lower dimensional material (LD) materials into PSC structure.<sup>23,25–31</sup> Among these approaches, LD material integration has emerged as a promising strategy and an extensively investigated approach in recent studies.<sup>6,22,32–34</sup>

LD materials including graphene-related materials (graphene, reduced graphene oxide (rGO), and graphene quantum dots (GQDs)), black phosphorus (BP), and transition metal dichalcogenides such as molybdenum disulfide (MoS<sub>2</sub>), tungsten disulfide (WS<sub>2</sub>), and tungsten diselenide (WSe<sub>2</sub>) have been identified as promising candidates to improve the thermal and chemical stability of PSCs.<sup>6,20,22,33–37</sup> Incorporating LD materials in different layers of PSCs (*e.g.*, electrode, charge transport layers, or as additives to the absorber layer), works as a good barrier for moisture and oxygen, restrains the migration of ions (from the perovskite into the metal electrode and *vice versa*), and improves thermal stability.<sup>6,37</sup> As such, LD materials have succeeded in increasing the stability of PSCs.<sup>33,37</sup> LD materials can also enhance the PCE of PSCs with their high carrier mobilities, tunable work function, transparency, and mechanical flexibility.<sup>22,33,37</sup> In addition, carbon-based materials have been investigated as potential alternatives for both front contact as a replacement for transparent conductive oxides and back contact (BC) for metal electrode replacement.<sup>6,37–39</sup> Graphene-based substrates were identified as excellent candidates for replacing the environmentally harmful indium in the fabrication of transparent conductive oxide-free flexible PSCs, making them most suitable for building integrated PV applications.<sup>6,22,38,40–42</sup> Utilizing carbon based electrodes used as the BC helps in developing hole transport layer (HTL) free and metal-free PSCs, paving the way for cost-effective, hydrophobic, thermally stable, highly efficient, and environmentally friendly PSC devices for future energy generation.<sup>6,11,21,22,39</sup>

While the research and development on enhancing the PCE and stability of PSC technology using LD material continues, it is also essential to identify the environmental impacts associated with PSC in the early stage of this technology's development. After conducting a comprehensive literature review, we have identified that assessments on environmental impacts, and commonly reported sustainability metrics (energy demand,

payback time, *etc.*) of LD material-based PSCs (ld-PSC) are missing. Furthermore, there is a lack of comparative analysis between the environmental performance of ld-PSCs and commercial PV technologies.

In this study, we identify the critical materials and processes that influence the environmental sustainability of ld-PSC for large-scale manufacturing. This is the first study incorporating a sustainability assessment tool such as life cycle assessment (LCA) method to layout the design and fabrication principles for the sustainable development of ld-PSC. First, we selected LD materials that are commonly incorporated into PSCs and have demonstrated significant enhancement in both stability and PCE. Subsequently, we identified the most scalable production methods for these LD materials for the integration of PSCs and modeled associated life cycle inventories for large-scale manufacturing of ld-PSCs. Our study encompasses two distinct alternative (Alt) ld-PSC configurations: Alt-1, which incorporates LD materials with lower environmental impacts at each layer, and Alt-2, which employs LD materials with relatively higher environmental impacts for each layer integration. Then, we compared the environmental performance of these two PSCs structures with that of reference PSCs without LD materials integration and commercial PV technologies including c-Si, copper indium gallium diselenide (CIGS), and cadmium telluride (CdTe). Following this comparative analysis, a sensitivity analysis was conducted to assess and compare the environmental performance of two alternative ld-PSC configurations with that of commercial PV technologies, considering a range of lifetime and PCE values. Additional analysis comparing the global warming potential (GWP) and energy payback time (EPBT) of these two alternative ld-PSC configurations with the reference PSC and established PV technologies is also included in the study.

## 2. Methods

### 2.1. Goal and scope

The goal of this study is to assess the environmental performance of ld-PSC in comparison to reference PSC and commercial PV technologies. The LCA was carried out in accordance with principles outlined in ISO 14040:2006<sup>43</sup> and ISO 14044:2006<sup>44</sup> guidelines. Additionally, we followed methodological guidelines provided by the international energy agency, which include recommendations for PV-specific technical aspects, life cycle inventory modeling, and life cycle impact assessment methods.<sup>45</sup> The results of this study will inform researchers and decision-makers in understanding the environmental performance of ld-PSC. Additionally, the findings from this study provide sustainable design principles for the commercialization of PSC technologies.

A cradle-to-end-of-use system boundary was selected, which includes raw material extraction, PSC manufacturing, and LD material deposition. We considered only electricity generation from ld-PSCs during operations phase and didn't consider maintenance required during operations. This ld-PSC



technology is still at the research stage and considered relatively new, which introduces a higher level of uncertainty in assessing end-of-life phases. Therefore, we exclude end-of-life phase from our analysis. The functional unit chosen for this LCA analysis was 1 kW h of electricity generated by ld-PSC in their lifetime. For LCA analysis, GaBi ts 10.0<sup>46</sup> software was used, and impact assessment was carried out using the tool for the reduction and assessment of chemicals (TRACI) 2.1<sup>47</sup> method. The ten midpoint impact categories of TRACI impact assessment method: acidification (kg SO<sub>2-eq.</sub>), ecotoxicity (CTU<sub>e</sub>), eutrophication (kg N<sub>eq.</sub>), GWP (kg CO<sub>2-eq.</sub>), human toxicity (CTU<sub>h</sub>), cancer and non-cancer, human health particular air (kg PM<sub>2.5-eq.</sub>), resources-fossil fuels (MJ<sub>surplus energy</sub>), ozone depletion (kg CFC11<sub>eq.</sub>), and smog (kg O<sub>3-eq.</sub>) were modeled. In addition, this study calculated the cumulative energy demand (CED) and energy payback time (EPBT)<sup>15</sup> for all the assessed PV technologies.

## 2.2. Selection of LD materials and their manufacturing processes for PSC integration

The reported experimental studies that incorporate LD materials into PSCs provided the baseline secondary data for this LCA study.<sup>48–57</sup> The summary of improvements in PV device parameters after the incorporation of LD materials into each layer is also provided in Table S.6 (ESI†). Recent literature shows that LD materials are mainly used to improve the stability and PCE of materials in electron transporting layer (ETL), absorber, and hole transporting layer (HTL) of regular PSCs. The commonly employed materials in the layers of reference PSC consist of SnO<sub>2</sub> for ETL, CH<sub>3</sub>NH<sub>3</sub>PbI<sub>3</sub> for absorber, and spiro-OMeTAD for HTL. Note that the utilization of spiro-OMeTAD in mass-scale production of PSC has concerns due to its high cost.<sup>11</sup> However, the current literature places significant emphasis on the integration of LD materials into this material<sup>53,54,57</sup> compared to low-cost HTL materials (see the ESI,† for our additional analysis based on a low-cost HTL alternative using copper thiocyanate (CuSCN)). Furthermore, the inverted PSC structure with poly(3,4-ethylenedioxythiophene)-polystyrene sulfonate

(PEDOT:PSS) as HTL and 6,6-phenylC61butyric acid methyl ester (PCBM) with LD materials integration<sup>58</sup> also assessed in ESI.†

The LD materials considered in this study were categorized into three groups: (1) graphene-related materials (graphene ink, rGO, and GQDs), (2) transition metal dichalcogenide (MoS<sub>2</sub>) (3) BP. Table 1 shows various LD materials that are incorporated into the PSC structure and their benefits over reference PSC. Previous literature shows that the incorporation of these LD materials into ETL, absorber, and HTL of PSC enhanced the PCE by more than 5% and retained >90% of the initial efficiencies when compared to the conventional PSC.<sup>48–54</sup> Despite the low cost and excellent mechanical stability, PSCs with carbon-based BC typically exhibit lower PCE values when compared to those utilizing metal back contacts.<sup>6,39</sup> As shown in Table 1, the incorporation of graphene as a BC for PSCs does not result in any enhancements in PCE when compared to the reference PSC using metal BC.<sup>39</sup> Similarly, the incorporation of graphene as a transparent conductive electrode did not yield any significant improvements in the PCE of ld-PSC.<sup>6,37,38</sup> Therefore, we focused our attention on integrating LD materials exclusively into the ETL, absorber, and HTL of PSC.

Fig. 1 shows the integration of LD materials into PSC's layers and possible manufacturing techniques for these LD materials. We went through a rigorous elimination process to identify the most scalable methods that can be used for the incorporation of LD materials with PV systems. We eliminated the processes that are energy and time intensive, and not cost effective. For example, graphene-related materials can be produced by exfoliation and chemical oxidation–reduction of graphite, and chemical vapor deposition methods. Among these production routes, exfoliation and chemical oxidation–reduction of graphite methods are most suited for commercial-scale production.<sup>59–61</sup> This is because chemical vapor deposition is an energy-intensive and expensive method.<sup>61</sup> Among exfoliation-based graphene synthesis routes, we chose electrochemical exfoliation using potassium hydroxide over the liquid exfoliation method because it yields high quality graphene

Table 1 Different LD materials integration into PSC structure and their benefits

| PSC layer      | LD material integration | Reported properties   | Ref. |
|----------------|-------------------------|---|------|
| ETL            | Graphene                | 15% increase in PCE and retaining 90% initial PCE values                  | 48   |
|                | GQDs                    | 24% increase in PCE and retaining 95% of initial PCE values               | 49   |
|                | BPQDs                   | 15% increase in PCE and retaining 90% of initial PCE values               | 55   |
| Absorber layer | BP-nano                 | 10% increase in PCE and retaining 94% of initial PCE values               | 56   |
|                | rGO                     | 30% increase in PCE and retaining 90% of initial PCE values               | 51   |
|                | GQDs                    | 10% increase in PCE and retaining 94% of initial PCE values               | 52   |
| HTL            | BP-nano                 | 25% increase in PCE and retaining 90% of initial PCE values               | 53   |
|                | MoS <sub>2</sub>        | 10% increase in PCE and retaining 75% of initial PCE values               | 54   |
|                | rGO                     | 5% increase in PCE and retaining 75% of initial PCE values                | 57   |
| BC             | Graphene                | Negligible improvements in PCE and retained 95% of its initial PCE values | 39   |

Note: In some of the studies where LD materials were integrated into absorber and HTL of PSC structures, TiO<sub>2</sub> was used as ETL instead of SnO<sub>2</sub>. These studies were still included in our analysis because the observed enhancements in the PCE and stability in this ld-PSC were primarily attributed to improvements in the absorber layer and HTL rather than the ETL





**Fig. 1** Various LD material integration into PSC structure and possible synthesis routes. The color-coded processes represent possible synthesis routes, with bold colored ones indicating the selected routes for LD materials in this study. The processes highlighted in grey color have been excluded from consideration due to their impracticality for commercial-scale production, as they are both energy and time-intensive.

sheets without using toxic solvents and is a simple process for commercial production.<sup>60,61</sup> Other graphene-related compounds, such as rGO and GQDs, are derived from graphene oxide (GO), which is produced by the chemical oxidation of graphite.<sup>62</sup> The chemical oxidation of graphite can be achieved by the modified hummers (Bangal variant) process.<sup>62</sup> The scalable production of GQDs from GO can be obtained using chemical oxidation and hydrothermal methods.<sup>63</sup> We chose the continuous hydrothermal approach developed by Kellici *et al.* for commercial-scale GQD manufacture since it is a rapid method and suitable for large-scale production.<sup>63,64</sup> For rGO synthesis, among chemical and thermal reduction methods, we chose the former because it is a cost-effective method for producing rGO on a large scale.<sup>61</sup> Among various synthesis routes for MoS<sub>2</sub> nanosheets, we chose the solvothermal method as a feasible solution for large-scale production.<sup>65</sup>

The solvothermal method for generating MoS<sub>2</sub> nanosheets is a low-temperature and one-step technique.<sup>65</sup> We found common methodologies for the production of BP-nano and black phosphorus quantum dots (BPQDs), such as electrochemical exfoliation and liquid phase exfoliation.<sup>50,66</sup> Because of its low cost and simple operational procedures, we chose liquid phase exfoliation as the most scalable approach for BP-nano and BPQDs.<sup>66</sup>

### 2.3. Life cycle inventories

The life cycle inventories were created using most recent data for mass-scaled PV production and experimental data for LD specific components. First, the materials and energy inventories for PSC, c-Si, CIGS, and CdTe modules were developed using the IEA-photovoltaic power systems (PVPS) TASK 12

**Table 2** Inventory for various LD materials and chemicals used for the dispersion of these LD materials into ETL, HTL, and absorber layers of PSCs. The mass of all the materials was calculated for 1 m<sup>2</sup> of the PSC module. DMF-dimethyl formamide, DMAc-dimethylacetamide, IPA-isopropyl alcohol

| Layer          | LD               | LD materials/chemicals | Mass | Units  | Comments  | Ref.          |
|----------------|------------------|------------------------|------|--|---|---------------|
| ETL            | Graphene         | Graphene               | 22.7 | mg   | 1 vol% of graphene in SnO <sub>2</sub> solution                     | 48 and 73     |
|                |                  | Ethanol                | 8.0  | g  | 1 g of graphene in 354 g ethanol                                    |               |
|                | GQDs             | GQD                    | 5.2  | mg   | 1 wt% of GQDs in SnO <sub>2</sub> solution                          | 74            |
|                |                  | Water                  | 5.3  | g  | 1 mg ml <sup>-1</sup> of GQDs in water                              |               |
|                | BPQDs            | BPQDs                  | 3    | mg   | SnO <sub>2</sub> with 1.5 Mm BPQDs concentration                    | 55            |
| Ethanol        |                  | 4.8                    | g    | 0.5 mg ml <sup>-1</sup> of BPQDs in ethanol        |   |               |
| Absorber layer | rGO              | rGO                    | 1.4  | g  | 0.14 mg of rGO doped into 645 mg of perovskite                      | 51            |
|                |                  | DMF                    | 6580 | g  | 0.2 mg ml <sup>-1</sup> of rGO in DMF                               |               |
|                | GQDs             | GQDs                   | 47   | mg   | GQDs concentration in perovskite solution is 7 vol%                 | 52            |
|                |                  | DMAc                   | 29.3 | g  | 0.93 g ml <sup>-1</sup> of GQDs in DMAc                             |               |
|                | BP-nano          | BP-nano                | 2.6  | mg   | Assumed 1 wt% of BP in perovskite solution                          | 56            |
| DMF            |                  | 2.5                    | g    | 0.1 mg ml <sup>-1</sup> of BP-nano in DMF          |   |               |
| HTL            | rGO              | rGO                    | 2.6  | mg   | Assumed 1 wt% of rGO in spiro-OMeTAD solution                       | 75            |
|                |                  | Chlorobenzene          | 1.45 | g  | 2 mg ml <sup>-1</sup> of rGO in chlorobenzene                       |               |
|                | BP-nano          | BP-nano                | 60   | mg   | 400 ml of BP solution with a concentration of 6 mg ml <sup>-1</sup> | 70            |
|                |                  | IPA                    | 8    | g  | 0.78 g ml <sup>-1</sup> of BP-nano in IPA                           |               |
|                | MoS <sub>2</sub> | MoS <sub>2</sub>       | 0.25 | g  | MoS <sub>2</sub> layer thickness is 50 nm                           | 54, 76 and 77 |
| IPA            |                  | 981                    | g    | 0.2 mg ml <sup>-1</sup> of MoS <sub>2</sub> in IPA |   |               |



report<sup>45</sup> as a baseline for manufacturing of a 1 m<sup>2</sup> PV panel. For ld-PSC configuration, the life cycle inventories were prepared by separately analyzing PSC production and LD material deposition. The synthesis of the PSC component involved sputtering the ETL onto FTO/glass, with subsequent deposition of the absorber layer and HTL deposited by slot die coating.<sup>67,68</sup> The metal electrode was then deposited using the evaporation method.<sup>67</sup> These studies were selected because they addressed deposition techniques that are suitable for large-scale production. Further, the inventories for incorporating LD materials into 1 m<sup>2</sup> of PSC were created based on literature.<sup>50–57</sup> Table 2 summarizes the quantities, type of chemical and specification for solvents used in the dispersion of these LD materials into unit area of PSCs. Furthermore, the material and energy required for the synthesis of graphene-related materials and MoS<sub>2</sub> were directly taken from the previous studies<sup>62,64,65,69</sup> whereas for BP production, we prepared the inventories based

on the previous experimental study.<sup>70</sup> All the inventories for the synthesis of unit mass of LD materials are shown in Table 3. All LCA models for all the PV technologies and LD materials were subsequently created using the GaBi software<sup>46</sup> and using the data from Ecoinvent V.3.8<sup>71</sup> database.

The lifetime and PCE of ld-PSC have varied in previous studies (see Table 1).<sup>21,35,36</sup> These studies found that ld-PSCs retained more than 80% of their initial PCE after 30–45 days, whereas control PSCs retained only 50%. The lifespan of both PSCs and ld-PSC was unknown, ranging from 1 to 25 years in the literature.<sup>72</sup> Given these uncertainties, the study made the following assumptions: the initial PCE of both the PSC and ld-PSC was set at 25%. The average lifetime PCE of ld-PSC is ~22%, taking into account an 80% retention of initial PCE, while reference PSC maintains an average PCE of ~19% with only 50% of their initial PCE retained. The projected lifespan for PSCs is 25 years, whereas ld-PSCs were assumed to

**Table 3** Material and energy inventories required for the production of 1 g of various LD materials

| LD materials     |        | Materials/energy               | Value | Units | Ref. |
|------------------|--------|--------------------------------|-------|-------|------|
| Graphene         | Output | Graphene dispersion            | 1     | g     | 62   |
|                  | Inputs | Anode, graphite                | 3.91  | g     |      |
|                  |        | Electricity, medium voltage    | 1.85  | MJ    |      |
|                  |        | Potassium hydroxide            | 1.12  | g     |      |
|                  |        | Water, deionized               | 670   | g     |      |
| GO               | Output | GO                             | 1     | g     | 62   |
|                  | Inputs | Electricity, medium voltage    | 0.01  | MJ    |      |
|                  |        | Graphite                       | 0.71  | g     |      |
|                  |        | Hydrogen peroxide (100%)       | 1.24  | g     |      |
|                  |        | Potassium permanganate         | 2.14  | g     |      |
|                  |        | Sodium nitrate                 | 0.36  | g     |      |
|                  |        | Sulfuric acid                  | 30    | g     |      |
|                  |        | Water, deionized               | 223   | g     |      |
| rGO              | Output | rGO                            | 1     | g     | 62   |
|                  | Inputs | GO                             | 1.25  | g     |      |
|                  |        | Electricity, medium voltage    | 0.38  | MJ    |      |
|                  |        | Ammonia                        | 0.34  | g     |      |
|                  |        | Methanol                       | 10    | g     |      |
|                  |        | Hydrazine                      | 1.40  | g     |      |
|                  |        | Water, deionized               | 163   | g     |      |
| GQDs             | Output | GQDs                           | 1     | mg    | 64   |
|                  | Inputs | GO                             | 20    | mg    |      |
|                  |        | Potassium hydroxide            | 440   | mg    |      |
|                  |        | Water, deionized               | 240   | g     |      |
|                  |        | Electricity, medium voltage    | 0.20  | kW h  |      |
| MoS <sub>2</sub> | Output | MoS <sub>2</sub>               | 1     | g     | 65   |
|                  | Inputs | Molybdenum                     | 1.14  | g     |      |
|                  |        | Hydrazine                      | 20.23 | g     |      |
|                  |        | Sodium hydroxide               | 11.52 | g     |      |
|                  |        | Elemental sulfur               | 0.52  | g     |      |
|                  |        | Ammonium carbonate             | 0.62  | g     |      |
|                  |        | Ethylenediamine                | 199   | g     |      |
|                  |        | Water, deionized               | 100   | g     |      |
|                  |        | Acetone                        | 150   | g     |      |
|                  |        | Electricity, medium voltage    | 0.01  | kW h  |      |
| BP-nano/BPQDs    | Output | BP-nano/BPQDs                  | 1     | g     | 53   |
|                  | Inputs | Bulk BP crystal                | 2.85  | g     |      |
|                  |        | <i>N</i> -Methyl pyrrolidinone | 1.42  | kg    |      |
|                  |        | Isopropyl alcohol              | 157   | g     |      |
|                  |        | Electricity, medium voltage    | 0.05  | kW h  |      |



experience a 15% increase in lifetime, extending to 28.75 years. The lifespan and PCE of Id-PSC values were uncertain which impacts the robustness of LCA results. To enhance the robustness of impact results, we performed a sensitivity analysis for both the PCE and lifetime. Given that the average PCE of the reference PSC is 19%, we explored a range of PCE values for Id-PSC starting from 19% (assuming no PCE improvement) and extended up to 27.5%. Additionally, we also explored a broad range of lifetimes for Id-PSC in sensitivity analysis, spanning from 5 to 35 years.

### 3. Results

#### 3.1. Environmental impacts comparison between LD materials

Fig. 2 shows the impacts of producing a unit mass of LD materials for four commonly reported environmental impact categories, namely GWP, CED, ecotoxicity, and human toxicity-cancer (see Table S.1 for all the remaining environmental impact categories, ESI<sup>†</sup>). Across all four assessed categories, GQDs and BP-nano show a significantly higher environmental impact while rGO and graphene have negligible impacts. For GQDs, over 90% of environmental impacts across four categories can be attributed to energy used in synthesis. This is because the direct electricity consumed in the continuous hydrothermal process is sourced from a single batch and for a small quantity of GQDs.<sup>64</sup> For BP-nano's environmental impacts, the synthesis of bulk BP crystals relies on white phosphorus, which contributes around 50% in all four impact categories. The impacts associated with white phosphorous are due to the substantial consumption of phosphate rock and electricity during the synthesis process. Following closely, the

second most significant factor contributing to the environmental impacts of BP-nano is the electricity consumption during the exfoliation and solvent exchange process of BP nanosheets, which varies between 30–35% across the four impact categories. The remaining 10–20% of BP-nano impacts in four impact categories are associated with the *N*-methyl pyrrolidone solvent used for the exfoliation of bulk BP crystals. The production of a unit mass of MoS<sub>2</sub> shows significantly lower environmental impacts than GQDs and BP-nano across all four impact categories. In terms of MoS<sub>2</sub>'s GWP, CED, and human toxicity/cancer impacts, the primary contributor is the ethylenediamine solvent used for the exfoliation of bulk BP crystals. The production of a unit mass of MoS<sub>2</sub> shows significantly lower environmental impacts than GQDs and BP-nano across all four impact categories. In terms of MoS<sub>2</sub>'s GWP, CED, and human toxicity/cancer impacts, the primary contributor is the ethylenediamine solvent used for the exfoliation of bulk BP crystals. The production of a unit mass of MoS<sub>2</sub> shows significantly lower environmental impacts than GQDs and BP-nano across all four impact categories. In terms of MoS<sub>2</sub>'s GWP, CED, and human toxicity/cancer impacts, the primary contributor is the ethylenediamine solvent used for the exfoliation of bulk BP crystals. The production of a unit mass of MoS<sub>2</sub> shows significantly lower environmental impacts than GQDs and BP-nano across all four impact categories. In terms of MoS<sub>2</sub>'s GWP, CED, and human toxicity/cancer impacts, the primary contributor is the ethylenediamine solvent used for the exfoliation of bulk BP crystals.

#### 3.2. Environmental impacts comparison between LD materials incorporated into PSCs

Two alternative (Alt) configurations of Id-PSC have been analyzed to discuss the environmental impacts of the integration of LD materials into the PSC. Alt-1 contains graphene in the ETL, BP in the absorber layer, and rGO in the HTL, and Alt-2 incorporates GQDs in the ETL, rGO in the absorber layer, and BP in the HTL. Fig. 3 shows the contributions of the average impacts resulting from the main components of Id-PSCs such as from PSC part and LD materials. We found that the impacts from LD materials incorporated into Alt-1 have a negligible contribution (<0.5%) to the overall impacts, whereas LD materials integrated into Alt-2 contributed to ~30% of the overall impacts. The substantial impact of LD materials in Alt-2 arises from both the considerable quantity of the LD materials integrated and chemicals used for the dispersion of these materials into Alt-2 configuration. For example, integration of rGO into the absorber layer of Alt-2 configuration requires a larger volume of DMF solvent during the dispersion process, accounting for 27% of the overall impacts of Alt-2 configuration. These impacts are predominantly linked to the organic compound dimethylamine, which is utilized in the synthesis of

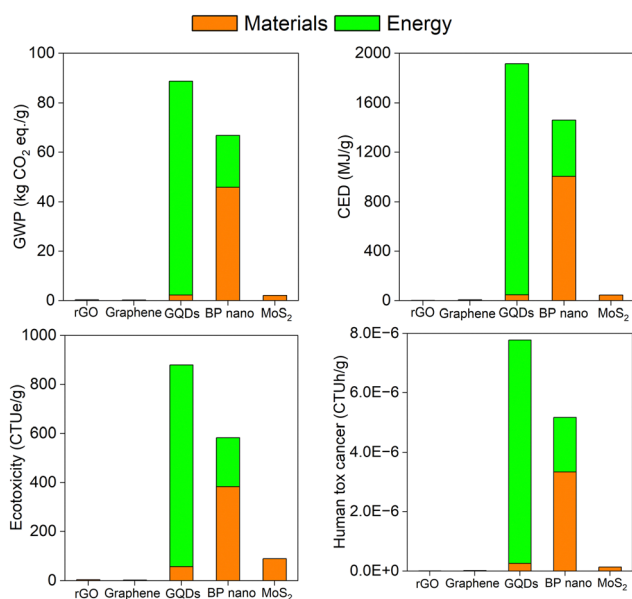


Fig. 2 Environmental impacts associated with materials and energy utilized in the synthesis of 1 g of various LD materials across GWP, CED, ecotoxicity, and human toxicity (cancer) categories.

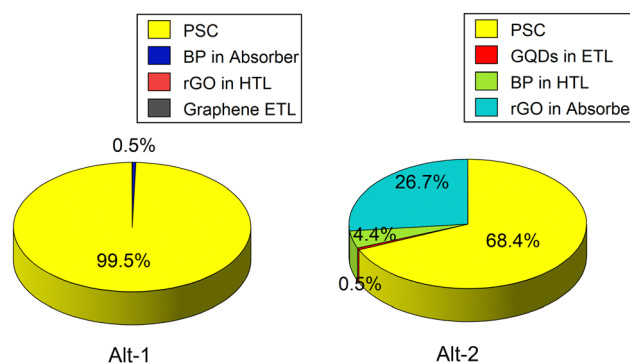


Fig. 3 The breakdown of environmental impacts by each component of Alt-1 and Alt-2 Id-PSC on overall average impacts. The environmental impacts of each component for 1 m<sup>2</sup> of the Id-PSC module were calculated for all impact categories. The average contribution of each component is calculated according to Celik *et al.*<sup>78</sup> The raw data for each component for 1 m<sup>2</sup> is also provided in Tables S.2–S.5 (ESI<sup>†</sup>).



**Table 4** Comparison of the normalized environmental impacts of PSCs with commercial PV technologies. The results are normalized with the environmental impacts of reference PSC technology. The raw data for remaining PV technologies can be extracted using representative multipliers derived from baseline data of reference PSC, as provided in the last column. The equation for converting 1 m<sup>2</sup> of impacts to kW h impacts is provided in eqn (S.1) (ESI).<sup>15</sup> The average normalized impacts were determined by taking the mean of ten impact categories, following an approach similar to Celik et al.<sup>78</sup> In the Alt-1 ld-PSC configuration, the ETL incorporates graphene, the absorber layer integrates BP, and the HTL involves rGO. The Alt-2 ld-PSC comprises the inclusion of GQDs in ETL, rGO in the absorber layer, and BP in HTL. Alternative HTL material *i.e.*, inorganic CuSCN-based ld-PSC configuration in comparison to Alt-1 configuration also assessed in Table S.8 (ESI). PCE and lifetime values of CdTe, CIGS, c-Si, and PSC are directly taken from PVPS TASK 12 report.<sup>45</sup> An additional comparison between Alt-1 and inverted ld-PSC configuration, integrated with LD materials is also presented in Table S.9 (ESI)

| PV technology                    | Commercial PV |             |             | Perovskite PV |             |             | PSC impacts/kW h                                 |
|----------------------------------|---------------|-------------|-------------|---------------|-------------|-------------|--|
|                                  | CdTe          | CIGS        | c-Si        | Alt-1         | Alt-2       | PSC         |  |
| PCE (%)                          | 18            | 16          | 20          | 22            | 22          | 19          |  |
| Lifetime (years)                 | 25            | 25          | 25          | 28.75         | 28.75       | 25          |  |
| Impact category                  |               |             |             |               |             |             |  |
| Acidification                    | 0.75          | 1.27        | 1.77        | 0.75          | 1.32        | 1.00        | $5.70 \times 10^{-5}$ (kg SO <sub>2</sub> -eq)   |
| Ecotoxicity                      | 0.39          | 0.63        | 1.08        | 0.75          | 0.79        | 1.00        | $9.62 \times 10^{-1}$ (CTUe)                     |
| Eutrophication                   | 0.79          | 0.72        | 2.77        | 0.76          | 1.20        | 1.00        | $4.06 \times 10^{-5}$ (kg N-eq)                  |
| GWP                              | 1.28          | 1.99        | 2.78        | 0.76          | 1.25        | 1.00        | $6.01 \times 10^{-3}$ (kg CO <sub>2</sub> -eq)   |
| Human health particulate air     | 1.21          | 1.34        | 2.74        | 0.76          | 1.04        | 1.00        | $1.34 \times 10^{-5}$ (kg PM <sub>2.5</sub> -eq) |
| Human toxicity, cancer           | 0.95          | 1.43        | 1.40        | 0.75          | 0.91        | 1.00        | $1.26 \times 10^{-9}$ (CTUh)                     |
| Human toxicity, non-canc.        | 0.24          | 0.45        | 1.04        | 0.75          | 0.82        | 1.00        | $1.02 \times 10^{-8}$ (CTUh)                     |
| Ozone depletion air              | 1.07          | 3.52        | 2.66        | 0.76          | 1.56        | 1.00        | $6.16 \times 10^{-10}$ (kg CFC 11-eq)            |
| Resources, fossil fuels          | 1.12          | 1.91        | 2.13        | 0.76          | 1.70        | 1.00        | $8.15 \times 10^{-3}$ (MJ surplus energy)        |
| Smog air                         | 0.82          | 1.62        | 1.68        | 0.75          | 0.98        | 1.00        | $6.56 \times 10^{-4}$ (kg O <sub>3</sub> -eq)    |
| <b>Average normalized impact</b> | <b>0.86</b>   | <b>1.50</b> | <b>2.00</b> | <b>0.75</b>   | <b>1.15</b> | <b>1.00</b> |  |
| <b>CED</b>                       | 1.22          | 1.68        | 2.72        | 0.76          | 1.50        | 1           | $1.10 \times 10^{-1}$ (MJ)                       |

|                                  |           |
|----------------------------------|-----------|
| Most environmentally preferable  | <0.70     |
| More environmentally preferable  | 0.71-0.85 |
| Neutral                          | 0.86-1.14 |
| Less environmentally preferable  | 1.15-1.29 |
| Least environmentally preferable | >1.30     |

DMF. This finding emphasizes the critical importance of carefully choosing the dispersion chemical for ld-PSC. The BP-nano integrated into HTL has moderate impacts on the environmental performance of Alt-2; this is due to an upstream process such as the white phosphorous consumption in the synthesis of bulk BP crystals. The incorporation of GQDs in ETL has the least contribution to the overall impacts from Alt-2 and these minor impacts are primarily associated with electricity utilized in the synthesis of GQDs. To sum up, these results indicate that Alt-1 employing graphene in the ETL, BP in the absorber layer, and rGO in the HTL is the most promising configuration for sustainable PSC design in future energy generation.

In Table 4, we compared the environmental performance of unit electricity generated from Alt-1 and Alt-2 systems with other commercial PV technologies and PSC, as well as provided a detailed analysis regarding the impacts of them each environmental category, captured in the US EPA TRACI. PSC is used as a reference point for this analysis. Our results show that Alt-1 has the lowest, and c-Si has the highest impacts among almost

all environmental categories which leads Alt-1 to be the most environmentally preferable PV structure, according to the average normalized environmental impacts. The environmental performance of Alt-1 is about ~25% and 40% better than PSC, and Alt-2, respectively. The improved environmental performance of Alt-1 compared to PSC is essentially a result of improvements in lifetime and PCE since the incorporation of LD materials into the PV structure has negligible impacts. The improved performance of Alt-1 compared to Alt-2 is a result of lower impacts, particularly in acidification, GWP, ozone depletion, eutrophication and resources, and fossil fuels categories. Alt-2 contains rGO in the absorber layer which contributes 30 to 50% of each of these categories. In addition, the white phosphorous that is necessary for the synthesis of BP-nano, which is integrated into HTL, contributes to the impacts of up to 7% across ozone depletion, eutrophication, resources, and fossil fuels categories. Next, the mass of rGO in the absorber layer, and BP-nano in the HTL overlayer of Alt-2 is nearly 20 times and 500 times more than the mass of BP-nano in the absorber layer



and rGO in HTL of Alt-1. Because of these significantly lower quantities of LD materials in HTL and absorber layers, Alt-1 has better environmental performance in all impact categories than Alt-2. Compared to commercial PV technologies, Alt-1 has significantly lower impacts in almost all impact categories except for ecotoxicity and human toxicity (non-cancer) categories, where CdTe and CIGS score better. The production of single-Si cells and aluminum alloy majorly contributed to significantly higher impacts of c-Si PV across all impact categories. In the context of CIGS, ozone depletion impacts are nearly four times higher compared to Alt-1. This notable increase in this impact category can be associated with polyethylene terephthalate used in the encapsulation of CIGS modules. The utilization of solar glass and aluminum alloy in CIGS is 1.5 to 2 times higher than the Alt-1 PSC configuration, which is responsible for higher impacts of CIGS compared to Alt-1 in the remaining impact categories. The adverse environmental performance of CdTe compared to Alt-1, is attributed to its higher impacts, especially in GWP, human health particularly air, ozone depletion and resources, and fossil fuel impact categories. The cause of these higher impacts in these categories is due to the higher electricity used in CdTe manufacturing (almost four times that of Alt-1). In addition, the improved environmental performance of Alt-1 compared to commercial PV technologies can also be attributed to enhanced PCE and extended lifetime resulting from the incorporation of LD materials.

### 3.3. Sensitivity analysis

To further explore the impacts of lifetime and PCE on the average normalized environmental impacts of Alt-1 and Alt-2 ld-PSC, we independently varied these parameters and pointed out the technological development in terms of PCE and lifetime that these PVs outperform conventional PVs and PSCs (Fig. 4). The findings from this analysis reveal that Alt-1 does not require any enhancement in terms of lifetime and PCE, whereas Alt-2 requires significant improvements in both lifetime and PCE to outperform the environmental performance of reference PSC and certain commercial PV technologies. For Alt-

2 ld-PSC to achieve an environmental impact equivalent to PSC, it would require a minimum of a 27 year lifetime and PCE of at least 27.5%. Similarly, to outperform the environmental performance of CdTe, Alt-2 ld-PSC would need a minimum lifetime of 31 years and a PCE of 27.5%.

Furthermore, it's worth noticing that Alt-1 ld-PSC can surpass the environmental performance of commercial PV technologies, even when functioning with reduced lifetimes (Fig. 4a). To determine the break-even lifetime of Alt-1 ld-PSC, the following equation is used:

$$\text{Impact}_{\text{Alt-1}} \times \frac{25}{\text{Lifetime}_{\text{Alt-1}}} = \text{Impact}_{\text{comm}} \quad (1)$$

where  $\text{Impact}_{\text{Alt-1}}$  and  $\text{Impact}_{\text{comm}}$  are the average normalized impact of the Alt-1 ld-PSC and commercial PV technologies, and  $\text{Lifetime}_{\text{Alt-1}}$  is the lifetime of Alt-1 ld-PSC. The commercial PV technology's lifetime is assumed to be 25 years. For example, Alt-1 ld-PSC with 20% PCE would need a lifetime of only 10.3, 13.8, and 24 years to outperform the environmental performance of c-Si, CIGS, and CdTe technologies respectively, which is currently shorter than the PSC lifetime (25 years). Therefore, the incorporation of LD materials like graphene in the ETL, BP in the perovskite layer, and rGO in HTL of Alt-1 demonstrates significant potential for the commercial applications of PSC. This is due to their ability to align with the environmental performance of PSC and commercial PV technologies, even within a shorter lifetime.

### 3.4. GWP impacts and EPBT: comparison with commercial PV technologies

The GWP impacts, also known as carbon footprint, and EPBT (see eqn (S2), ESI<sup>†</sup>) values of electricity generated from ld-PSC, along with a comparative analysis against PSC and commercial PV technologies are shown in Fig. 5. Overall, Alt-1 ld-PSC has lower GWP and EPBT values than PSC and commercial PV technologies. The GWP impacts of various PV technologies range from ~4.5 to 17 g CO<sub>2eq</sub>. per kW h. Among the various PV technologies analyzed, Alt-1 ld-PSC exhibits lower GWP impacts, while c-Si PV shows comparatively higher GWP impacts.

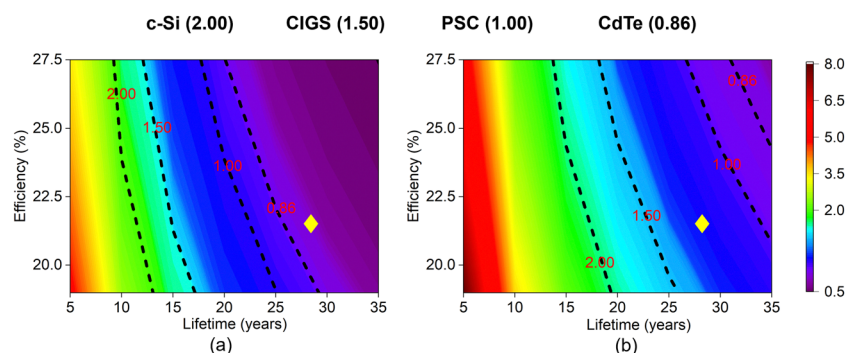


Fig. 4 The influence of PCE and lifetime on the average normalized environmental impacts of Alt-1 (a) and Alt-2 (b) ld-PSC. The diamond icon (yellow) represents the average normalized environmental impact of Alt-1 ld-PSC (i.e., 0.76) and Alt-2 ld-PSC (1.16), corresponding to the current lifetime and PCE. The average normalized environmental impact of c-Si, CdTe, and CIGS is 2.00, 0.86, and 1.50 respectively (as outlined in Table 4). Additionally, Fig. 4a and b also show the environmental impact of ld-PSC equivalent to PSC and commercial technologies in black dashed lines.





The GWP impact of Alt-1 ld-PSC is 4.5 g CO<sub>2eq.</sub> per kW h, which is ~20–40% lower than PSC and Alt-2 ld-PSC technologies, and ~40–75% lower than commercial PV technologies. We further compared the GWP impacts of PSC and commercial PV technologies with recent literature findings. Leccisi *et al.* reported GWP impacts of PSC, CdTe, and CIGS PV technologies in terms of m<sup>2</sup> of PV panels.<sup>9</sup> To facilitate a meaningful comparison with our study, we converted these GWP impacts from m<sup>2</sup> to kW h impacts, assuming comparable irradiation levels, PCE, performance ratio, and lifetime parameters as used in our study. The GWP impacts of PSC, CdTe, and CIGS technologies as calculated according to Leccisi *et al.* were 5.3, 9.0, and 18.5 g CO<sub>2eq.</sub> per kW h, respectively. The GWP values obtained for PSC and commercial PV technologies in our study show slight variations when compared to the findings reported by Leccisi *et al.* Specifically, our study reveals that the GWP impacts of PSC technology are approximately 15% higher than the values documented by Leccisi *et al.* This disparity can be attributed to the utilization of different materials and deposition methods during the synthesis of PSC. For instance, in the study conducted by Leccisi *et al.*, they examined PSC structure utilizing CuSCN as HTL and molybdenum coupled with aluminum as BC. They employed a spray coating deposition method for PSC fabrication. In contrast, our study involves spiro-OMeTAD as HTL and silver as BC, with a slot die coating method used as a deposition method. For c-Si impacts, we compared our study results with the most recent LCA study conducted by Fthenakis *et al.*, which employed updated c-Si PV data.<sup>8</sup> Fthenakis reported a GWP of 22 g CO<sub>2eq.</sub> per kW h for c-Si, which is ~35% higher than the GWP impacts found in our study (17 g CO<sub>2eq.</sub> per kW h).<sup>8</sup> This is because we used a United States electricity mix source compared to the Chinese electricity mixture used in Fthenakis *et al.* Note that according to TRACI method, the GWP impacts of 1 kW h of electricity production in the US and China are calculated to be 0.4 and 0.9 kg CO<sub>2eq.</sub> per kW h, respectively, this difference could be responsible for disparities between our study findings and theirs.

The EPBT value of ld-PSC varies from approximately three to six months, whereas commercial technologies range from four

to nine months (Fig. 5). The Alt-1 ld-PSC has the lowest EPBT (2.8 months) among the analyzed PV technologies, while c-Si PV requires around nine months. The EPBT values of commercial PV technologies determined in this study are slightly lower compared to the findings from Leccisi *et al.* and Fthenakis *et al.*<sup>8,9</sup> This variation can be attributed to the embedded energy used in the EPBT calculations, which varies based on factors such as the materials and deposition methods used in synthesis, the country specific electricity mixes and associated characterization factors.

## 4. Conclusions

In this study, we considered five LD materials that are frequently investigated for the integration of PSC: graphene, rGO, GQDs, MoS<sub>2</sub>, and BP. A unit mass-based LD materials comparison reveals that rGO, graphene, and MoS<sub>2</sub> are the most environmentally friendly options. However, the environmental impact of these materials undergoes significant when integrated into ld-PSC configurations, depending on the type and quantity of chemicals used for the dispersion. This emphasizes the critical importance of carefully choosing the chemicals used for dispersion. For the assessment of the environmental performance of ld-PSC following the incorporation of various LD materials, we selected two distinct ld-PSC configurations and conducted a comparative analysis with reference PSC and commercial PV technologies. Our results show that Alt-1 ld-PSC configuration which incorporates graphene in the ETL, BP in perovskite, and rGO in HTL layers has ~20% lower average environmental impacts compared to PSC. Conversely, the Alt-2 ld-PSC configuration that employs GQDs in ETL, rGO in the absorber layer, and BP in the HTL layer showed ~15% more average impacts than PSC. Furthermore, this study also highlighted that Alt-1 ld-PSC configuration operating at a benchmark PCE of 20%, demonstrated the potential to outperform c-Si, CIGS, and CdTe technologies at a lower lifetime of only 10.3, 13.8, and 24 years, respectively. Moreover, the investigation of significant sustainability metrics, such as energy payback time, demonstrated that with ld-PSC, the energy can be paid back in a time period up to three times shorter than commercial PV technologies. The findings of the study emphasize the significance of Alt-1 ld-PSC as a sustainable PSC configuration that can outperform established commercial PV technologies.

## Conflicts of interest

There are no conflicts to declare.

## Acknowledgements

This work is partially funded by the US National Science Foundation's Grants # 2138293 and 2239755. We thank Dr Venkata Ramana Gadhamshetty for his valuable comments in the initial phase of the development of this work.



Fig. 5 Comparison of GWP and EPBT of Alt-1 and Alt-2 ld-PSC with reference PSC and other commercial PV technologies. These comparisons are made under the assumption of an average global solar irradiation of 1700 kW h m<sup>-2</sup> year<sup>-1</sup>, and a performance ratio of 0.75.



## References

- International Energy Agency, *Snapshot of Global PV Markets 2023. Task 1 Strategic PV Analysis and Outreach*. IEA PVPS, Paris, France, 2023, vol. I.
- International Energy Agency, *Tracking SDG7: The Energy Progress Report 2023*, Paris, France, 2023.
- Statista, Global solar energy share in electricity mix 2022, <https://www.statista.com/statistics/1302055/global-solar-energy-share-electricity-mix/>, (accessed 30 October 2023).
- DNV, Energy Transition Outlook – 2023, <https://www.dnv.com/energy-transition-outlook/index.html>, (accessed 1 November 2023).
- J. Pastuszak and P. Węgierek, Photovoltaic Cell Generations and Current Research Directions for Their Development, *Materials*, 2022, **15**, 5542.
- S. Suragtkhuu, S. Sunderiya, P. Mygmarsereejid, S. Purevdorj, A. S. R. Bati, B. Bold, Y. L. Zhong, S. Davaasambuu and M. Batmunkh, Graphene-Like Monoelemental 2D Materials for Perovskite Solar Cells, *Adv. Energy Mater.*, 2023, **13**, 2204074.
- National Renewable Energy Laboratory (NREL), Best Research-Cell Efficiency Chart | Photovoltaic Research | NREL, <https://www.nrel.gov/pv/cell-efficiency.html>, (accessed 17 October 2023).
- V. Fthenakis and E. Leccisi, Updated sustainability status of crystalline silicon-based photovoltaic systems: life-cycle energy and environmental impact reduction trends, *Prog. Photovoltaics Res. Appl.*, 2021, **29**, 1068–1077.
- E. Leccisi and V. Fthenakis, Life cycle energy demand and carbon emissions of scalable single-junction and tandem perovskite PV, *Prog. Photovoltaics Res. Appl.*, 2021, **29**, 1078–1092.
- A. Maalouf, T. Okoroafor, Z. Jehl, V. Babu and S. Resalati, A comprehensive review on life cycle assessment of commercial and emerging thin-film solar cell systems, *Renewable Sustainable Energy Rev.*, 2023, **186**, 113652.
- I. Celik, Z. Song, A. J. Cimaroli, Y. Yan, M. J. Heben and D. Apul, Life Cycle Assessment (LCA) of perovskite PV cells projected from lab to fab, *Sol. Energy Mater. Sol. Cells*, 2016, **156**, 157–169.
- J. Y. Kim, J.-W. Lee, H. S. Jung, H. Shin and N.-G. Park, High-Efficiency Perovskite Solar Cells, *Chem. Rev.*, 2020, **120**, 7867–7918.
- J. Zhang, N. Chang, C. Fagerholm, M. Qiu, L. Shuai, R. Egan and C. Yuan, Techno-economic and environmental sustainability of industrial-scale productions of perovskite solar cells, *Renewable Sustainable Energy Rev.*, 2022, **158**, 112146.
- N. Kwon, J. Lee, M. J. Ko, Y. Y. Kim and J. Seo, Recent progress of eco-friendly manufacturing process of efficient perovskite solar cells, *Nano Converge.*, 2023, **10**, 1–18.
- I. Celik, A. B. Phillips, Z. Song, Y. Yan, R. J. Ellingson, M. J. Heben and D. Apul, Environmental analysis of perovskites and other relevant solar cell technologies in a tandem configuration, *Energy Environ. Sci.*, 2017, **10**, 1874–1884.
- P. Čulík, K. Brooks, C. Momblona, M. Adams, S. Kinge, F. Maréchal, P. J. Dyson and M. K. Nazeeruddin, Design and Cost Analysis of 100 MW Perovskite Solar Panel Manufacturing Process in Different Locations, *ACS Energy Lett.*, 2022, 3039–3044.
- I. Celik, R. Hosseinian Ahangharnejhad, Z. Song, M. Heben and D. Apul, Emerging Photovoltaic (PV) Materials for a Low Carbon Economy, *Energies*, 2020, **13**, 4131.
- J. Zheng, W. Duan, Y. Guo, Z. C. Zhao, H. Yi, F. J. Ma, L. Granados Caro, C. Yi, J. Bing, S. Tang, J. Qu, K. C. Fong, X. Cui, Y. Zhu, L. Yang, A. Lambertz, M. Arafat Mahmud, H. Chen, C. Liao, G. Wang, M. Jankovec, C. Xu, A. Uddin, J. M. Cairney, S. Bremner, S. Huang, K. Ding, D. R. McKenzie and A. W. Y. Ho-Baillie, Efficient monolithic perovskite-Si tandem solar cells enabled by an ultra-thin indium tin oxide interlayer, *Energy Environ. Sci.*, 2023, **16**, 1223–1233.
- A. W. Y. Ho-Baillie, J. Zheng, M. A. Mahmud, F. J. Ma, D. R. McKenzie and M. A. Green, Recent progress and future prospects of perovskite tandem solar cells, *Appl. Phys. Rev.*, 2021, **8**, DOI: [10.1063/5.0061483](https://doi.org/10.1063/5.0061483).
- A. S. R. Bati, M. Batmunkh and J. G. Shapter, Emerging 2D Layered Materials for Perovskite Solar Cells, *Adv. Energy Mater.*, 2020, **13**, 1902253.
- M. Alzaid, Recent progress in the role of two-dimensional materials as an efficient charge transport layer in perovskite solar cells, *Int. J. Energy Res.*, 2021, **45**, 12598–12613.
- S. O. Ali Ahmad, A. Ashfaq, M. U. Akbar, M. Ikram, K. Khan, F. Wang, M. Ikram and A. Mahmood, Application of two-dimensional materials in perovskite solar cells: recent progress, challenges, and prospective solutions, *J. Mater. Chem. C*, 2021, **9**, 14065–14092.
- C. C. Boyd, R. Checharoen, T. Leijtens and M. D. McGehee, Understanding Degradation Mechanisms and Improving Stability of Perovskite Photovoltaics, *Chem. Rev.*, 2019, **119**, 3418–3451.
- D. Zhang, D. Li, Y. Hu, A. Mei and H. Han, Degradation pathways in perovskite solar cells and how to meet international standards, *Commun. Mater.*, 2022, **3**, 58.
- G. Jeong, D. Koo, J. Seo, S. Jung, Y. Choi, J. Lee and H. Park, Suppressed interdiffusion and degradation in flexible and transparent metal electrode-based perovskite solar cells with a graphene interlayer, *Nano Lett.*, 2020, **20**, 3718–3727.
- S. Wu, R. Chen, S. Zhang, B. H. Babu, Y. Yue, H. Zhu, Z. Yang, C. Chen, W. Chen, Y. Huang, S. Fang, T. Liu, L. Han and W. Chen, A chemically inert bismuth interlayer enhances long-term stability of inverted perovskite solar cells, *Nat. Commun.*, 2019, **10**, 1–11.
- M. Dehghanipour, A. Behjat and H. Amrollahi Bioki, Fabrication of stable and efficient 2D/3D perovskite solar cells through post-treatment with TBABF<sub>4</sub>, *J. Mater. Chem. C*, 2021, **9**, 957–966.
- A. R. Bin Mohd Yusoff, M. Vasilopoulou, D. G. Georgiadou, L. C. Palilis, A. Abate and M. K. Nazeeruddin, Passivation and process engineering approaches of halide perovskite films for high efficiency and stability perovskite solar cells, *Energy Environ. Sci.*, 2021, **14**, 2906–2953.
- S. Tang, S. Peracchi, Z. Pastuovic, C. Liao, A. Xu, J. Bing, J. Zheng, M. A. Mahmud, G. Wang, E. D. Townsend-Medlock,



- G. J. Wilson, G. Lakhwani, C. Brenner, D. R. McKenzie and A. W. Y. Ho-Baillie, Effect of Hole Transport Materials and Their Dopants on the Stability and Recoverability of Perovskite Solar Cells on Very Thin Substrates after 7 MeV Proton Irradiation, *Adv. Energy Mater.*, 2023, **13**, 1–9.
- 30 C. A. R. Perini, E. Rojas-Gatjens, M. Ravello, A. F. Castro-Mendez, J. Hidalgo, Y. An, S. Kim, B. Lai, R. Li, C. Silva-Acuña and J. P. Correa-Baena, Interface Reconstruction from Ruddlesden–Popper Structures Impacts Stability in Lead Halide Perovskite Solar Cells, *Adv. Mater.*, 2022, **34**, 2204726.
- 31 C. A. R. Perini, A. F. Castro-Mendez, T. Kodalle, M. Ravello, J. Hidalgo, M. Gomez-Dominguez, R. Li, M. Taddei, R. Giridharagopal, J. Pothoof, C. M. Sutter-Fella, D. S. Ginger and J. P. Correa-Baena, Vapor-Deposited  $n = 2$  Ruddlesden–Popper Interface Layers Aid Charge Carrier Extraction in Perovskite Solar Cells, *ACS Energy Lett.*, 2023, **8**, 1408–1415.
- 32 T. Dai, Q. Cao, L. Yang, M. H. Aldamasy, M. Li, Q. Liang, H. Lu, Y. Dong and Y. Yang, Strategies for high-performance large-area perovskite solar cells toward commercialization, *Crystals*, 2021, **11**, 295.
- 33 U. K. Aryal, M. Ahmadpour, V. Turkovic, H. G. Rubahn, A. Di Carlo and M. Madsen, 2D materials for organic and perovskite photovoltaics, *Nano Energy*, 2022, **94**, 106833.
- 34 M. Hadadian, J. H. Smått and J. P. Correa-Baena, The role of carbon-based materials in enhancing the stability of perovskite solar cells, *Energy Environ. Sci.*, 2020, **13**, 1377–1407.
- 35 P. You, G. Tang and F. Yan, Two-dimensional materials in perovskite solar cells, *Mater. Today Energy*, 2019, **11**, 128–158.
- 36 N. E. Safie, M. A. Azam, M. F. A. Aziz and M. Ismail, Recent progress of graphene-based materials for efficient charge transfer and device performance stability in perovskite solar cells, *Int. J. Energy Res.*, 2021, **45**, 1347–1374.
- 37 Z. Niazi, A. Hagfeldt and E. K. Goharshadi, Recent progress on the use of graphene-based nanomaterials in perovskite solar cells, *J. Mater. Chem. A*, 2023, **11**, 6659–6687.
- 38 J. H. Heo, D. S. Lee, F. Zhang, C. Xiao, S. J. Heo, H. J. Lee, K. Zhu and S. H. Im, Super Flexible Transparent Conducting Oxide-Free Organic–Inorganic Hybrid Perovskite Solar Cells with 19.01% Efficiency (Active Area = 1 cm<sup>2</sup>), *Sol. RRL*, 2021, **5**, 2100733.
- 39 Y. Wang, W. Li, Y. Yin, M. Wang, W. Cai, Y. Shi, J. Guo, W. Shang, C. Zhang, Q. Dong, H. Ma, J. Liu, W. Tian, S. Jin, J. Bian and Y. Shi, Defective MWCNT Enabled Dual Interface Coupling for Carbon-Based Perovskite Solar Cells with Efficiency Exceeding 22%, *Adv. Funct. Mater.*, 2022, **32**, 2204831.
- 40 J. Yoon, H. Sung, G. Lee, W. Cho, N. Ahn, H. S. Jung and M. Choi, Superflexible, high-efficiency perovskite solar cells utilizing graphene electrodes: towards future foldable power sources, *Energy Environ. Sci.*, 2017, **10**, 337–345.
- 41 A. S. R. Bati, Y. L. Zhong, P. L. Burn, M. K. Nazeeruddin, P. E. Shaw and M. Batmunkh, Next-generation applications for integrated perovskite solar cells, *Commun. Mater.*, 2023, **4**, 1–24.
- 42 J. Bing, L. G. Caro, H. P. Talathi, N. L. Chang, D. R. McKenzie and A. W. Y. Ho-Baillie, Perovskite solar cells for building integrated photovoltaics—glazing applications, *Joule*, 2022, **6**, 1446–1474.
- 43 ISO 14040:2006, Environmental management: Life cycle assessment; Principles and framework, <https://www.iso.org/standard/37456.html>, (accessed 7 September 2023).
- 44 ISO 14044:2006, Environmental management: Life cycle assessment; Requirements and guidelines, <https://www.iso.org/standard/38498.html>, (accessed 6 September 2023).
- 45 R. Frischknecht, P. Stolz, L. Krebs, M. de Wild-Scholten, P. Sinha, V. Fthenakis, C. Kim, M. Rauegi and M. Stucki, *Life Cycle Inventories and Life Cycle Assessments of Photovoltaic Systems. International Energy Agency (IEA) PVPS Task12, Report T12-19*, 2020.
- 46 Sphera, Life Cycle Assessment Software. LCA for Experts (GaBi), <https://sphera.com/life-cycle-assessment-lca-software/>, (accessed 7 September 2023).
- 47 J. Bare, *Tool for the Reduction and Assessment of Chemical and Other Environmental Impacts (TRACI). User's Guide Tool for the Reduction and Assessment of Chemical and Other Environmental Impacts (TRACI)*, Washington, DC, USA, 2012, vol. 600/R-12/5.
- 48 M. Zhu, W. Liu, W. Ke, L. Xie, P. Dong and F. Hao, Graphene-Modified Tin Dioxide for Efficient Planar Perovskite Solar Cells with Enhanced Electron Extraction and Reduced Hysteresis, *ACS Appl. Mater. Interfaces*, 2019, **11**, 666–673.
- 49 N. A. A. Malek, N. Alias, A. A. Umar, X. Zhang, X. Li, S. K. M. Saad, N. A. Abdullah, H. Zhang, Z. Weng, Z. Shi, C. Li, M. M. Rosli and Y. Zhan, Enhanced Charge Transfer in Atom-Thick 2H-WS<sub>2</sub> Nanosheets' Electron Transport Layers of Perovskite Solar Cells, *Sol. RRL*, 2020, **4**, 2000260.
- 50 R. Gui, H. Jin, Z. Wang and J. Li, Black phosphorus quantum dots: Synthesis, properties, functionalized modification and applications, *Chem. Soc. Rev.*, 2018, **47**, 6795–6823.
- 51 A. K. Kadhim, M. R. Mohammad and A. I. Abd Ali, Enhancing the efficiency of perovskite solar cells by modifying perovskite layer with rGO additive, *Chem. Phys. Lett.*, 2022, **786**, 2–6.
- 52 X. Fang, J. Ding, N. Yuan, P. Sun, M. Lv, G. Ding and C. Zhu, Graphene quantum dot incorporated perovskite films: Passivating grain boundaries and facilitating electron extraction, *Phys. Chem. Chem. Phys.*, 2017, **19**, 6057–6063.
- 53 S. K. Muduli, E. Varrla, S. A. Kulkarni, G. Han, K. Thirumal, O. Lev, S. Mhaisalkar and N. Mathews, 2D black phosphorous nanosheets as a hole transporting material in perovskite solar cells, *J. Power Sources*, 2017, **371**, 156–161.
- 54 A. Agresti, S. Pescetelli, A. L. Palma, B. Martín-García, L. Najafi, S. Bellani, I. Moreels, M. Prato and F. Bonaccorso, and A. Di Carlo, Two-Dimensional Material Interface Engineering for Efficient Perovskite Large-Area Modules, *ACS Energy Lett.*, 2019, **4**, 1862–1871.
- 55 B. Gu, Y. Du, B. Chen, R. Zhao, H. Lu, Q. Xu and C. Guo, Black Phosphorus Quantum Dot-Engineered Tin Oxide Electron Transport Layer for Highly Stable Perovskite Solar Cells with Negligible Hysteresis, *ACS Appl. Mater. Interfaces*, 2022, **14**, 11264–11272.



- 56 Y. Wang, H. Zhang, T. Zhang, W. Shi, M. Kan, J. Chen and Y. Zhao, Photostability of MAPbI<sub>3</sub> Perovskite Solar Cells by Incorporating Black Phosphorus, *Sol. RRL*, 2019, **3**, 1900197.
- 57 S. Suragtkhuu, O. Tserendavag, U. Vandandoo, A. S. R. Bati, M. Bat-Erdene, J. G. Shapter, M. Batmunkh and S. Davasambuu, Efficiency and stability enhancement of perovskite solar cells using reduced graphene oxide derived from earth-abundant natural graphite, *RSC Adv.*, 2020, **10**, 9133–9139.
- 58 W. Chen, K. Li, Y. Wang, X. Feng, Z. Liao, Q. Su, X. Lin and Z. He, Black Phosphorus Quantum Dots for Hole Extraction of Typical Planar Hybrid Perovskite Solar Cells, *J. Phys. Chem. Lett.*, 2017, **8**, 591–598.
- 59 P. You, G. Tang and F. Yan, Two-dimensional materials in perovskite solar cells Two-dimensional materials in perovskite solar cells, *Mater. Today Energy*, 2018, **11**, 128–158.
- 60 A. A. Moosa and M. S. Abed, Graphene preparation and graphite exfoliation, *Turkish J. Chem.*, 2021, **45**, 493–519.
- 61 N. Kumar, R. Salehiyan, V. Chauke, O. Joseph Botlhoko, K. Setshedi, M. Scriba, M. Masukume and S. Sinha Ray, Top-down synthesis of graphene: a comprehensive review, *FlatChem*, 2021, **27**, 100224.
- 62 M. Cossutta, J. McKechnie and S. J. Pickering, A comparative LCA of different graphene production routes, *Green Chem.*, 2017, **19**, 5874–5884.
- 63 C. Zhao, X. Song, Y. Liu, Y. Fu, L. Ye, N. Wang, F. Wang and L. Li, *Synthesis of graphene quantum dots and their applications in drug delivery*, 2020.
- 64 S. Kellici, J. Acord, K. E. Moore, N. P. Power, V. Middelkoop, D. J. Morgan, T. Heil, P. Coppo, I. A. Baragau and C. L. Raston, Continuous hydrothermal flow synthesis of graphene quantum dots, *React. Chem. Eng.*, 2018, **3**, 949–958.
- 65 M. Hachhach, H. Akram, A. El Kasmi, M. Hanafi, O. Achak and T. Chafik, Life cycle assessment of large-scale production of MoS<sub>2</sub> nanomaterials through the solvothermal method, *J. Nanoparticle Res.*, 2022, **24**, 1–14.
- 66 Y. Zeng and Z. Guo, Synthesis and stabilization of black phosphorus and phosphorene: Recent progress and perspectives, *iScience*, 2021, **24**, 103116.
- 67 M. de Wild-Scholten, Deliverable 3.1-Life Cycle Analysis of CHEOPS technologies and bench-marking: Screening, benchmarking, 2017, **3**, 1.
- 68 L. Ramseier, P. Stolz and R. Frischknecht, *Life Cycle Assessment of a Perovskite Silicon Tandem Photo-voltaic Panel*. Swiss Federal Office of Energy SFOE, Uster, Switzerland, 2019.
- 69 M. Cossutta, V. Vretenar, T. A. Centeno, P. Kotrusz, J. McKechnie and S. J. Pickering, A comparative life cycle assessment of graphene and activated carbon in a supercapacitor application, *J. Cleaner Prod.*, 2020, **242**, 118468.
- 70 S. K. Muduli, E. Varrla, S. A. Kulkarni, G. Han, K. Thirumal, O. Lev, S. Mhaisalkar, N. Mathews, K. Mahmood, A. Khalid, S. W. Ahmad, H. G. Qutab, M. Hameed, R. Sharif, F. A. Deorsola, N. Russo, G. A. Blengini, D. Fino, B. Gu, Y. Du, B. Chen, R. Zhao, H. Lu, Q. Xu and C. Guo, Black Phosphorus Quantum Dot-Engineered Tin Oxide Electron Transport Layer for Highly Stable Perovskite Solar Cells with Negligible Hysteresis, *J. Power Sources*, 2017, **203**, 1–6.
- 71 Ecoinvent, Ecoinvent v3.8, <https://ecoinvent.org/the-ecoinvent-database/data-releases/ecoinvent-3-8/>, (accessed 10 September 2023).
- 72 Z. Song, C. L. McElvany, A. B. Phillips, I. Celik, P. W. Krantz, S. C. Waththage, G. K. Liyanage, D. Apul and M. J. Heben, A technoeconomic analysis of perovskite solar module manufacturing with low-cost materials and techniques, *Energy Environ. Sci.*, 2017, **10**, 1297–1305.
- 73 S. Pescetelli, A. Agresti, G. Viskadourous, S. Razza, K. Rogdakis, I. Kalogerakis, E. Spiliariotis, E. Leonardi, P. Mariani, L. Sorbello, M. Pierro, C. Cornaro, S. Bellani, L. Najafi, B. Martín-García, A. E. Del Rio Castillo, R. Oropesa-Nuñez, M. Prato, S. Maranghi, M. L. Parisi, A. Sinicropi, R. Basosi, F. Bonaccorso, E. Kymakis and A. Di Carlo, Integration of two-dimensional materials-based perovskite solar panels into a stand-alone solar farm, *Nat. Energy*, 2022, **7**, 597–607.
- 74 J. Xie, K. Huang, X. Yu, Z. Yang, K. Xiao, Y. Qiang, X. Zhu, L. Xu, P. Wang, C. Cui and D. Yang, Enhanced Electronic Properties of SnO<sub>2</sub> via Electron Transfer from Graphene Quantum Dots for Efficient Perovskite Solar Cells, *ACS Nano*, 2017, **11**, 9176–9182.
- 75 S. Suragtkhuu, O. Tserendavag, U. Vandandoo, A. S. R. Bati, M. Bat-erdene, J. G. Shapter, M. Batmunkh and S. Davasambuu, Efficiency and stability enhancement of perovskite solar cells using reduced graphene oxide derived, *RSC Adv.*, 2020, **10**, 9133–9139.
- 76 L. L. Jiang, Z. K. Wang, M. Li, C. H. Li, P. F. Fang and L. S. Liao, Flower-like MoS<sub>2</sub> nanocrystals: A powerful sorbent of Li<sup>+</sup> in the Spiro-OMeTAD layer for highly efficient and stable perovskite solar cells, *J. Mater. Chem. A*, 2019, **7**, 3655–3663.
- 77 A. Capasso, F. Matteocci, L. Najafi, M. Prato, J. Buha, L. Cinà, V. Pellegrini, A. Di Carlo and F. Bonaccorso, Few-Layer MoS<sub>2</sub> Flakes as Active Buffer Layer for Stable Perovskite Solar Cells, *Adv. Energy Mater.*, 2016, **6**, 1–12.
- 78 I. Celik, B. E. Mason, A. B. Phillips, M. J. Heben and D. Apul, Environmental Impacts from Photovoltaic Solar Cells Made with Single Walled Carbon Nanotubes, *Environ. Sci. Technol.*, 2017, **51**, 4722–4732.

